Wan, X., Xiong, C., Wang, H., Zhang, K., Zheng, Z., He, Y., Yu, L. (2019): A Statistical Study on the Climatology of the Equatorial Plasma Depletions Occurrence at Topside Ionosphere During Geomagnetic Disturbed Periods. - *Journal of Geophysical Research*, *124*, 10, pp. 8023—8038.

DOI: http://doi.org/10.1029/2019JA026926

JGR Space Physics

RESEARCH ARTICLE
10.1029/2019JA026926

A Statistical Study on the Climatology of the Equatorial Plasma Depletions Occurrence at Topside Ionosphere During Geomagnetic Disturbed Periods

Xin Wan[1], Chao Xiong[2], Hui Wang[1], Kedeng Zhang[1], Zhichao Zheng[1], Yangfan He[1], and Lei Yu[1]

[1]College of Electronic Information, Wuhan University, Wuhan, China, [2]GFZ, German Research Centre for Geosciences, Potsdam, Germany

Key Points:

- The EPDs occurrence during 181 geomagnetic storms is statistically investigated via a superposed epoch analysis, for different season and local times
- Postsunset EPDs occurrence tends to be suppressed/enhanced at longitudes where the EPD normally prevails globally, except that at mid-Asia during June Solstice
- The storm-induced EPDs at predawn sector is more related to the fossil ones rather than fresh ones

Correspondence to:
X. Wan and H. Wang,
iml_wobscene@whu.edu.cn;
h.wang@whu.edu.cn

Citation:
Wan, X., Xiong, C., Wang, H., Zhang, K., Zheng, Z., He, Y., & Yu, L. (2019). A statistical study on the climatology of the Equatorial Plasma Depletions occurrence at topside ionosphere during geomagnetic disturbed periods. *Journal of Geophysical Research: Space Physics*, *124*, 8023–8038. https://doi.org/10.1029/2019JA026926

Received 7 MAY 2019
Accepted 26 AUG 2019
Accepted article online 13 SEPT 2019
Published online 24 OCT 2019

Abstract Using the in situ measurements of ROCSAT-1 satellite during 181 geomagnetic storms happened from July 1999 to June 2004, a superposed epoch analysis of the equatorial plasma depletions (EPDs) occurrence is conducted. At postsunset hours (1800–2200 LT), the EPDs occurrence is enhanced shortly at the storm onset, but afterward, a long-last suppression dominates. The EPDs occurrence at Midnight (2200–0200 LT) generally shares a similar pattern to that at postsunset hours. The occurrence at predawn (0200–0400) gradual increases near storm onset and reach its maximum at 6–9 hr and decays until 18 hr. For a given longitude at postsunset/midnight, the EPDs occurrence tends to be suppressed or promoted when the EPDs do or do not prevail. The disturbed vertical plasma drift generally determines the inhibition/promotion of the EPDs occurrence at postsunset/predawn. However, for predawn EPDs occurrence, the plasma vertical drift cannot well explain the longitudinal variation. The continuous observations from consecutive orbits of ROCSAT-1 are carefully compared and the result suggests that the geomagnetic storm-induced additional predawn EPDs are preferred to be the longer-lived developed EPDs rather than fresh EPDs. In addition, a possible mechanism concerning the background plasma density enhancement which might be related with the energetic electrons induced nighttime ionization is proposed.

1. Introduction

Equatorial plasma depletions (EPDs) represent an inhomogeneous distribution of plasma densities in the equatorial ionosphere after sunset hours. The generation and development of EPDs are explained by the generalized Rayleigh-Taylor (R-T) instability (e.g., Kelly, 2009; Sultan, 1996). The equatorial ionosphere at postsunset hours is unstable due to the rapid absence of sunlight. A steep upward plasma density gradient forms from the ionospheric E region where the recombination rate is higher, toward the F region where the recombination rate is much lower. The upward $\boldsymbol{E} \times \boldsymbol{B}$ drifts (e.g., Burke, Gentile, et al., 2004; Burke, Huang, et al., 2004; Stolle et al., 2008; Su et al., 2006; Xiong et al., 2012) are recognized as one of the primary factors for modulating the R-T instability growth rate, along with seeding mechanisms like gravity waves (e.g., Krall et al., 2013; McClure et al., 1998; Taori et al., 2011) and traveling ionosphere disturbances (e.g., Batista et al., 2006; Horvath & Lovell, 2010; Krall et al., 2011), to facilitate the generation and development of the EPDs. The influence of meridional neutral wind has also been discussed, as it can affect the F region peak height and modify the field line-integrated conductivities (e.g., Dao et al., 2017; Huba & Krall, 2013; Krall et al., 2009; Maruyama et al., 2009).

Due to the disturbances in the equatorial electric field and neutral wind circulations, EPDs occurrence during geomagnetic storms differs in climatology from that during geomagnetic quiet periods (e.g., Abdu, 2012; Abdu et al., 2012; Fejer et al., 2008b; Li et al., 2010; Smith & Heelis, 2018; Yeh et al., 2001). The disturbed electric fields could be categorized as the prompt penetration electric field (PPEF), which is characterized by the interplanetary magnetic field (IMF) B_z when its polarization turns from northward to southward (e.g., Senior & Blanc, 1984); the PEF which occurs when the IMF B_z turning northward from southward (e.g., Kelley et al., 1979); the disturbance wind dynamo electric field (DDEF) which is caused by the enhanced equatorward propagating disturbance winds induced by the energy input at high latitudes (e.g., Blanc & Richmond, 1980). The local time dependence of the disturbed electric field further leads to the local time dependence of the EPDs occurrence. The short-lived PPEF is eastward in the day time and westward at

night with the same orientation as the quiet time zonal electric field and has a life span of less than 2 hr. In contrast, the PEF and the DDEF has an opposite polarity with the quiet time zonal electric field; latter is usually observed several hours after the storm onset and even persisting for longer than 1 day (e.g., Fejer et al., 2008b). Abdu (2012) summarized that the postsunset/postmidnight EPDs (referred as spread *F* in their literature) can develop from PPEF/PEF, while it can be disrupted by PEF/PPEF, and EPDs only occur at the post-midnight sector when the DDEF dominates (Abdu et al., 2012).

However, at low-latitude and equatorial region, the response of ionospheric electric field to the geomagnetic storms could be much complicated, which is not in the uniform pattern as described in Abdu (2012). Xiong et al. (2015) found that the peak of the disturbance winds can corotate from 2300 to 0300 local time (LT) as they propagate from high to middle and low latitudes. Zhang et al. (2017) further provided observations that the DDEF could also be shifted to later local times. Hairston et al. (2013) showed a persistent enhanced downward plasma vertical drift at dayside and early evening hours through all phases of the 26 September 2011 storm, suggesting a total absence of the prompt penetration electric field. Tulasi et al. (2012) presented evidence that the disturbed electric field is in opposite polarization in equatorial *E* and *F* regions.

Besides the disturbed electric fields, the precipitation of energetic particles during storm periods has been also reported to contribute to the ionospheric disturbances. Yadav et al. (2011) reported that the ionospheric *F* layer was lifted over the Indian region, which was accompanied by decreased O^+ and increased H^+ concentrations during 31 March 2001 storm. The energetic particle (H^+/H) from the ring current and the consequent charge exchange reaction was suggested as the responsible mechanism. Abdu et al. (2008) suggested that the conductance enhancement produced by energetic particle induced ionization in the South Atlantic Anomaly (SAA) region is responsible for the abnormal fast upward plasma drift which favors the fountain effects as well as the EPDs occurrence. On the other hand, Burke, Gentile, et al. (2004) reported that the EPB occurrence at the west coast of South America is significantly lower than that of the east coast, and the longitudinal gradient of EPB occurrence is attributed to the enhanced E region Pederson conductivity associated with energetic particle induced ionization. Carter et al. (2016) reported the occurrence of post-midnight EPDs at the east coast of South America with the absence of DDEF during the recovery phase of 2015 St. Patrick's Day storm. The redistribution of plasma to higher altitude is found to be the main cause. However, the reason why the redistribution occurs has not been well explained. How does the disturbed EPDs occurrence vary with longitudes and in which way the EPDs occur differently associated with energetic particles are still open questions?

In addition, the ionospheric responses are quite different during different geomagnetic storms. Therefore, it is worth to investigate how the EPDs occurrence varies during geomagnetic storm from a statistical point of view. In this study, we presented a superposed epoch analysis (SEA) of the time evolution of EPDs occurrence during 181 geomagnetic storms by using in situ plasma density measurements of the ROCSAT-1 satellites. The season, local time, and longitudinal dependences of EPDs occurrence are discussed. Along with the ion vertical drift and ion density data, we analyzed the climatology of the EPDs occurrence, particularly for those occurs at predawn sector. For the first time, our analysis suggests that the geomagnetic storm-induced more predawn EPDs are preferred to be the longer-lived developed EPDs rather than developing (fresh) EPDs. Scenarios are proposed on the background plasma density enhancement which favors the sustainable development/maintenance of the EPDs, which benefits the EPDs occurrence at predawn sector during geomagnetic disturbed periods. Moreover, the preferential longitudes where occurs the background plasma density enhancement lies from east Pacific to SAA region, we suggest that the ionization induced by quasi-trapped energetic electrons (Suvorova et al., 2013, 2014, 2016) contributes. In the following, we first describe our data set and data processing method in section 2, then the statistical analysis is present in section 3; the discussion with previous relevant studies are provide in section 4.

2. Data Set and Approach

2.1. Data Set

ROCSAT-1 satellite was launched on 27 January 1999 and ended its mission on 17 June 2004. The satellite flew eastward at 630 km with an inclination of 35°, and the orbital period was 97 min. The ion number density (*Ni*) and ion vertical drift (meridional component perpendicular to the magnetic field, V_z) measured by Ionospheric Plasma and Electrodynamics Instrument (Yeh et al., 1999) in a time resolution of 1 s are used in this study.

In order to reproduce the reliable feature of V_z, several processes are conducted before the analysis to fix the V_z to a constant altitude, 600 km over the equator (Fejer et al., 2008a, 2008b; Lei et al., 2014). Data within ±15° dip latitude when the ion density was larger than 5×10^4 cm^3 are firstly sorted out; the selected V_z is secondly mapped to the apex height under the assumption that the electric field is equipotential along the magnetic field lines (Murphy & Heelis, 1986); the apex height was calculated using an approximate formula: $= \frac{alt+Re}{cos^2 diplat} - Re$ (*alt*: altitude; *Re*: earth radius; and *diplat*: dipole latitude). Note that as the apex height increases, the geomagnetic field strength decrease with $(H_{apex}+Re)^{-3}$ and the V_z at apex height (V_{apex}) was then normalized to that at 600 km over dip equator via the formula: $V_{alt=600Km} = V_{apex} \cdot \frac{(600+Re)^3}{(H_{apex}+Re)^3}$.

In addition, the ROCSAT-1 satellite visits the same longitude for two consecutive orbits with the latitude deviated in few degrees at off-equator to 10° at the equator (see orbit plotting in Figure 4). This special orbit configuration guarantees continuous observations during time interval of hours for a fixed longitudinal sector and makes it reliable to conduct a SEA of the ROCSAT-1 data.

2.2. EPD Detections

We use a similar algorithm to identify EPDs from the ion density measured by FORMOSA-1, which has earlier been applied to the Swarm electron density measurements as described in Wan et al. (2018). Briefly, we mark all the depletion regions along the *Ni* profile and record the depletion depths. Depletions which are not qualified to our algorithm are then excluded, for example, the qualification standard is set with few thresholds, the longitude gap of the depletion should be larger than 0.1° and smaller than 3°, the absolute depletion depth should be larger than 4×10^{10} m^{-3}, the relative depletion depth should be larger than 20%. Readers are suggested for more detailed description in section 2 of Wan et al. (2018).

2.3. The Superposed Epoch of Geomagnetic Storms

We use the *SYM-H* index to identify the different phases of geomagnetic storms. The first drop of *SYM-H* index (right after the sudden commencement or the gradual commencement) is first defined to mark the onset of the storm main phase. For the storms with more than one drop of *SYM-H* index, each drop is then treated as an individual indicator of the onset of each event. For example, Figure 1 shows the interplanetary and geomagnetic conditions of 13 October 2000 storm which contains two main phases. The vertical black dash line in Figure 1a marks the first onset of the storm when the solar wind dynamic pressure starts to increase and the IMF B_z turns to the southward, and the quiet time before the storm onset is presented with green lines. According to our definition, two gradual drops of *SYM-H* indicated by the red color (in the third panel) suggest two main storm phases and the two recovery phases occurring right after main phases are colored in blue. For the superposed analysis, we set the epoch at the onset of two main phases as marked as $\Delta t = 00$ hr.

Based on the coronal mass ejection driven geomagnetic storm lists as sorted by Jian et al. (2006), 181 events are determined during ROCSAT-1 life period. The superposed *SYM-H* index and Interplanetary Magnetic Field B_z component are presented in Figure 1b; the mean value of the indices is also presented as a black solid curve. By looking at the season, there are 71 events in equinoxes (March, April, September, and October), 68 near December solstice (December S., short for January, February, November, and December), 42 near June Solstice (June S., short for May–Aug).

3. Results

3.1. SEA on the EPDs Occurrence

The left column of Figure 2 shows the occurrence rate of EPDs as a function of the superposed epoch time. Note that the plotting is made in 1-hr step, and we set a time window of 5 hr for slide moving to guarantee the number of satellite orbit samples. The occurrence rate of EPDs is defined as the ratio between the satellite pass with EPDs detected and the total pass number during all the storm cases. We divided the EPDs events into three categories by their LT: postsunset (1800–2200 LT), midnight (2200–0200 LT), and predawn (0200–0600 LT). In addition, as the occurrence of EPDs has prominent seasonal dependence, the events have been further divided into three seasons as defined in section 2.3.

Before the epoch at $\Delta t = 00$ hr, the occurrence rate of EPDs at Midnight is comparable to that at postsunset hours for December solstice (Figure 2a). However, the occurrence rate of EPDs is generally increased/decreased from postsunset to midnight for June solstice/equinoxes (Figures 2b/2c), respectively. Similar results have been reported by previous studies (e.g., Carter et al., 2013; Stolle et al., 2008; Wan et al., 2018) that the occurrence rate of the EPDs increases rapidly after sunset and generally peaks before 0000 LT for December solstice and equinoxes, this local time evolution is delayed during June Solstice which leads to the highest probability of the occurrence of EPDs occurs near midnight. The Pre–Reversal Enhancement (PRE) was found also to peak at the later local time and decays slower in June solstice compared to the other two seasons (Fejer et al., 2008a; Stolle et al., 2008), which is possibly the reason to cause such seasonal/local time variation of the EPDs occurrence.

As the Δt approaches 00 hr, clear storm effects on the EPDs occurrence start to appear and last for the next 18 hr or even longer. That is, the occurrence rate of EPDs temporary increases near $\Delta t = 00$ hr and then decreases for the next 10 epoch hours at postsunset and midnight but shows prominent enhancement during predawn. The time evolution of EPDs occurrence also shows slight differences in seasons. For example, for postsunset and midnight sectors, the EPDs occurrence peaks earlier (at about $\Delta t = 2$ hr) during June solstice than that during December solstice (at about $\Delta t = 5$ hr). For predawn sector, the peak appears earlier (at about $\Delta t = 6$ hr) during December solstice than that during June solstice and equinoxes (at about $\Delta t = 9$ hr).

To better visualize the storm effects on the EPDs occurrence, we calculated the residual value regards to the EPDs occurrence under magnetic quiet periods. The EPDs occurrence during −72 to −24 and 48 to 96 hr (not plotted in Figure 2) is set as the reference. The residual occurrence is plotted in the Figures 2d–2f and labeled as residual occurrence rate. For the local time sector of postsunset and midnight, the residual plot (Figures 2d–2f) show that the EPDs occurrence generally experiences the short-duration enhancement during the first couple of hours except that at postsunset during equinoxes. Following the short-duration enhancement, the EPDs occurrence is getting significantly inhibited which can last for more than 18 hr.

For predawn sector, the significant enhancement after $\Delta t = 00$ hr can be clearly witnessed on both absolute plot as well as the residual plot which is also a consistent phenomenon throughout 00–18 hr during all the seasons. Slight seasonal variation can be identified that the EPDs occurrence peaks at $\Delta t = 06$ hr during December solstice which is about 3 hr earlier than that during June solstice and equinoxes.

Figure 3 shows the vertical plasma drift velocity (V_z), plotted in the same way as Figure 2. Stolle et al. (2008) reported that there is a 2- to 3-hr time lag between the PRE with the equatorial spread F occurrence at the topside ionosphere. Thus, three local time sectors for V_z have been adjusted to 1600–2000, 2000–0000, and 0000–0400 LT in respect to postsunset, midnight, and predawn which are set for the analysis of EPDs occurrence. In the following paragraphs, we still described 1600–2000/2000–0000/0000–0400 LT as postsunset/midnight/predawn. Concerning the uncertainty of the derived variations we obtain typical values for standard deviation (σ) of about 20 m/s for vertical plasma drift at each Δt point, which is quite large. More important for our analysis is the uncertainty of mean value. It is defined as σ/n, where n is the number of events contributing to each Δt point. From Figures 3, we see that the derived evolutions of perturbations in vertical plasma drift statistically significant, clearly larger than the uncertainty of mean value (error bar).

Maximum/minimum of V_z at 1600–2000/0000–0400 LT can always be witnessed near the epoch $\Delta t = 00$ hr, while V_z at 2000–2400 LT does not show a uniform pattern. This could be explained by the local time dependent of the PPEF induced disturbed vertical drift, that is, the disturbed upward V_z transit its polarization from positive to negative overnight from sunset to dawn, and the transition happens before midnight (Fejer et al., 2008b). Thus, the integrated disturbed V_z is upward/downward during 1600–2000/0000–0400 LT, while the polarization of disturbed V_z could be ambiguity during 2000–2400 LT. A long-duration inhibition/enhancement subsequently dominates for more than 24 hr after $\Delta t = 00$ hr for postsunset/predawn, which is also independent on the seasons. Nevertheless, it shows no such seasonal independent discipline when it comes to the V_z of Midnight sector, the evolution tendency of which is ambiguity. Similar to PPEF, DDEF changed its polarization at about 2200 LT for all three seasons (Fejer et al., 2008b), which might be the reason that V_z evolution of midnight sector is less regular in the epoch time series.

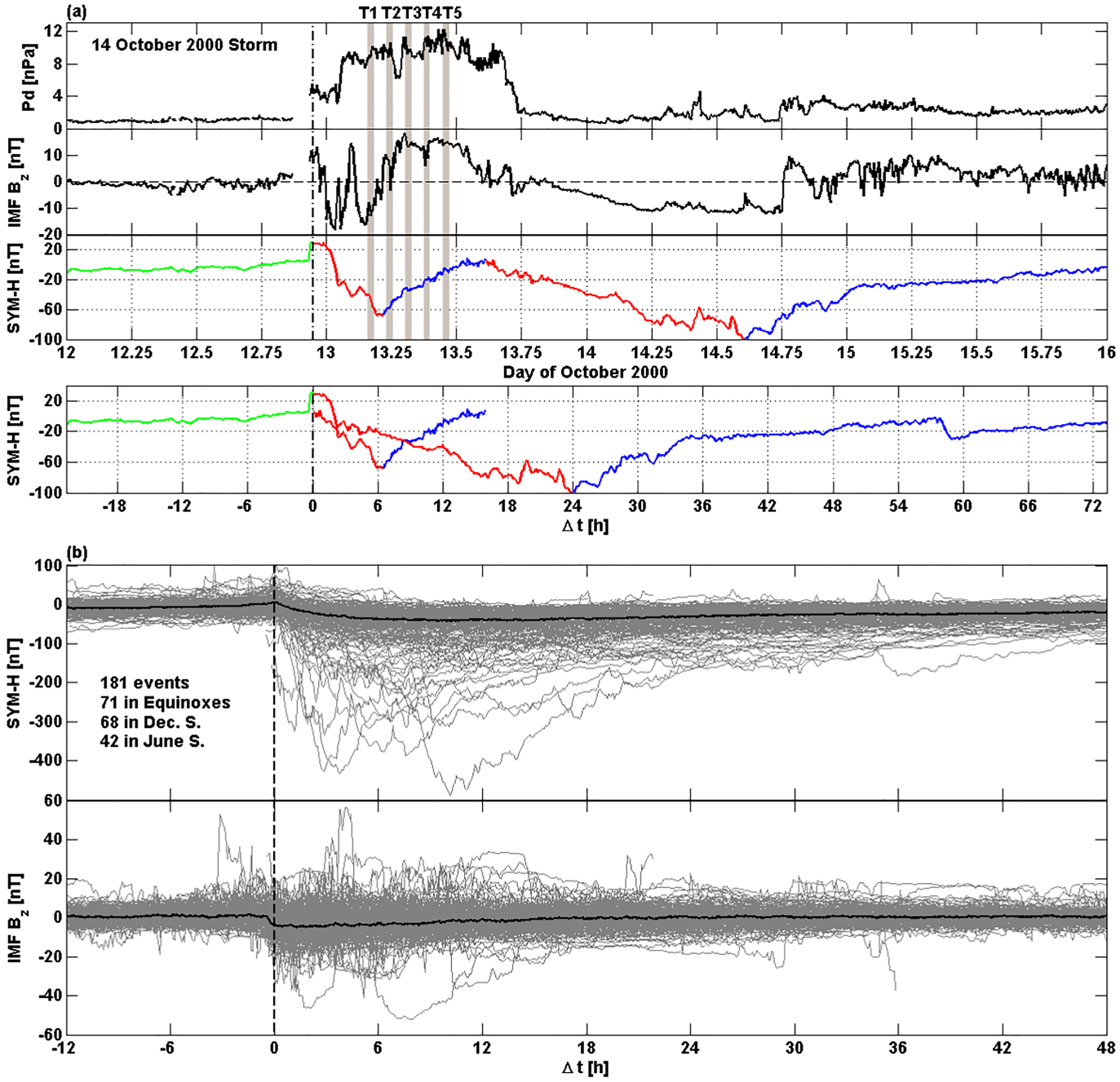

Figure 1. (a) Interplanetary and geomagnetic indices of 13 October 2000 storm and schematic of *SYM-H* based superimposing when the storm contains two main phases; (b) superposed storm time sequences based on 181 storm main phase events, the black curve is the mean value. The 0 hr mark the onset of the storms.

Same processes as introduced above were conducted to get the residual V_z (ΔV_z), shown in Figures 3d–3f. ΔV_z at postsunset/predawn generally recurrence the enhancement/inhibition near $\Delta t = 00$ hr during June solstice (Figure 3e) and equinoxes (Figure 3f), as well as the long-duration reversed trends after $\Delta t = 00$ hr which last for at least 30 hr. ΔV_z at Midnight shows the dependence on the seasons, that is, consider the Δt of 00–30 hr, midnight ΔV_z transit from negative to positive at $\Delta t = 14$ hr for June solstice while it stays in positive for equinoxes.

For December solstice (Figure 3d), ΔV_z is still positive during 00–30 hr for 0000–0400 LT which is consistent with that for the other two seasons. During the same epoch time period, ΔV_z stays in zero for 1600–2000 LT and positive for 2000–2400 LT, which is different from the signals of V_z in Figure 3a as well as ΔV_z in

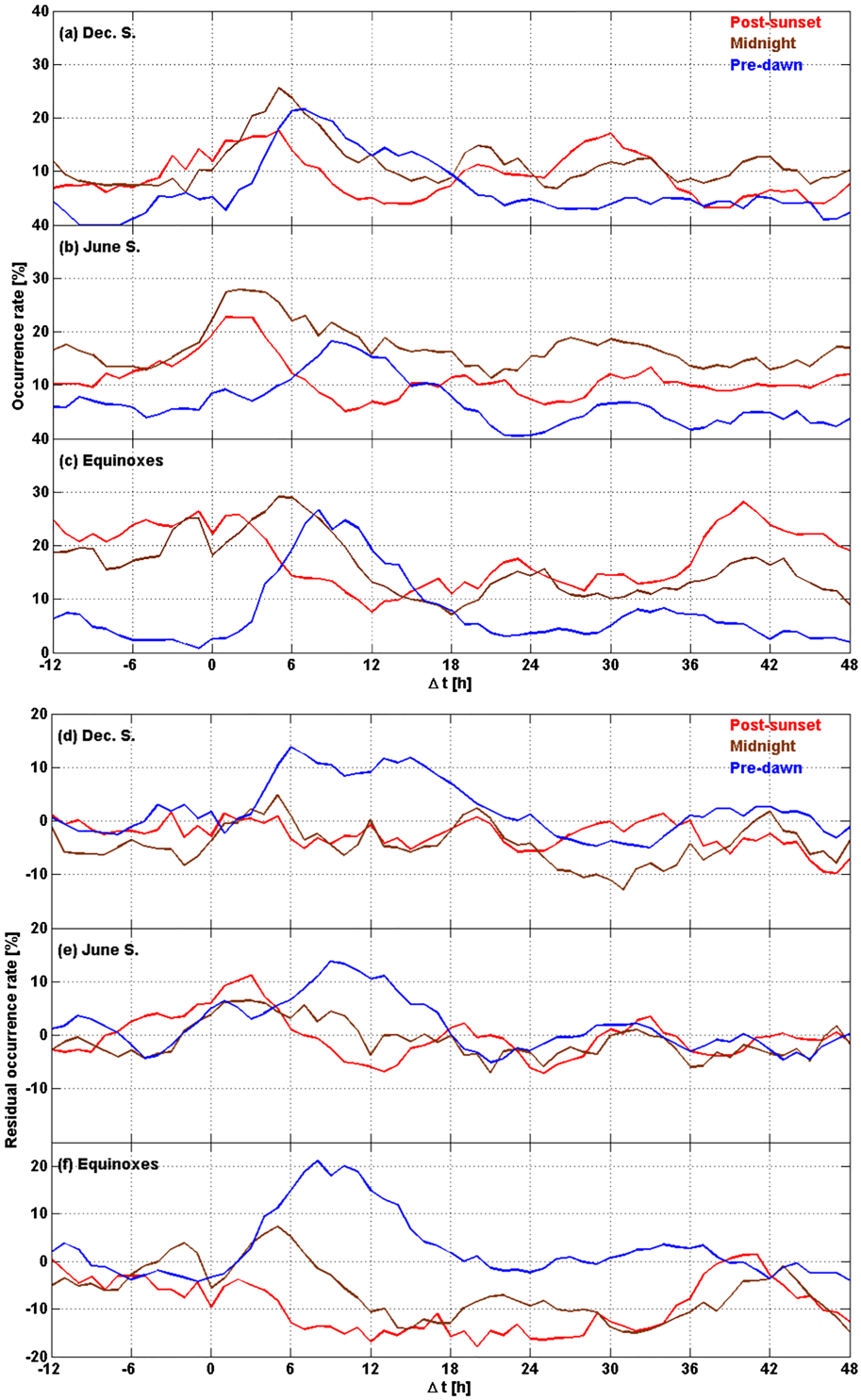

Figure 2. The superposed occurrence rate of EPDs, (a–c) absolute value and (d–f) residual values after removing referential occurrence rate of EPDs.

Figures 3e and 3f. However, we note that for the time period before 0 hr, ΔV_z already shows a large deviation from 0 m/s, the ΔV_z variation during December solstice is less convincing in this sense. Correlations between the occurrence rate of EPDs with V_z could be identified from the SEA while the disagreements also exist; the detailed analysis will be given in section 4.

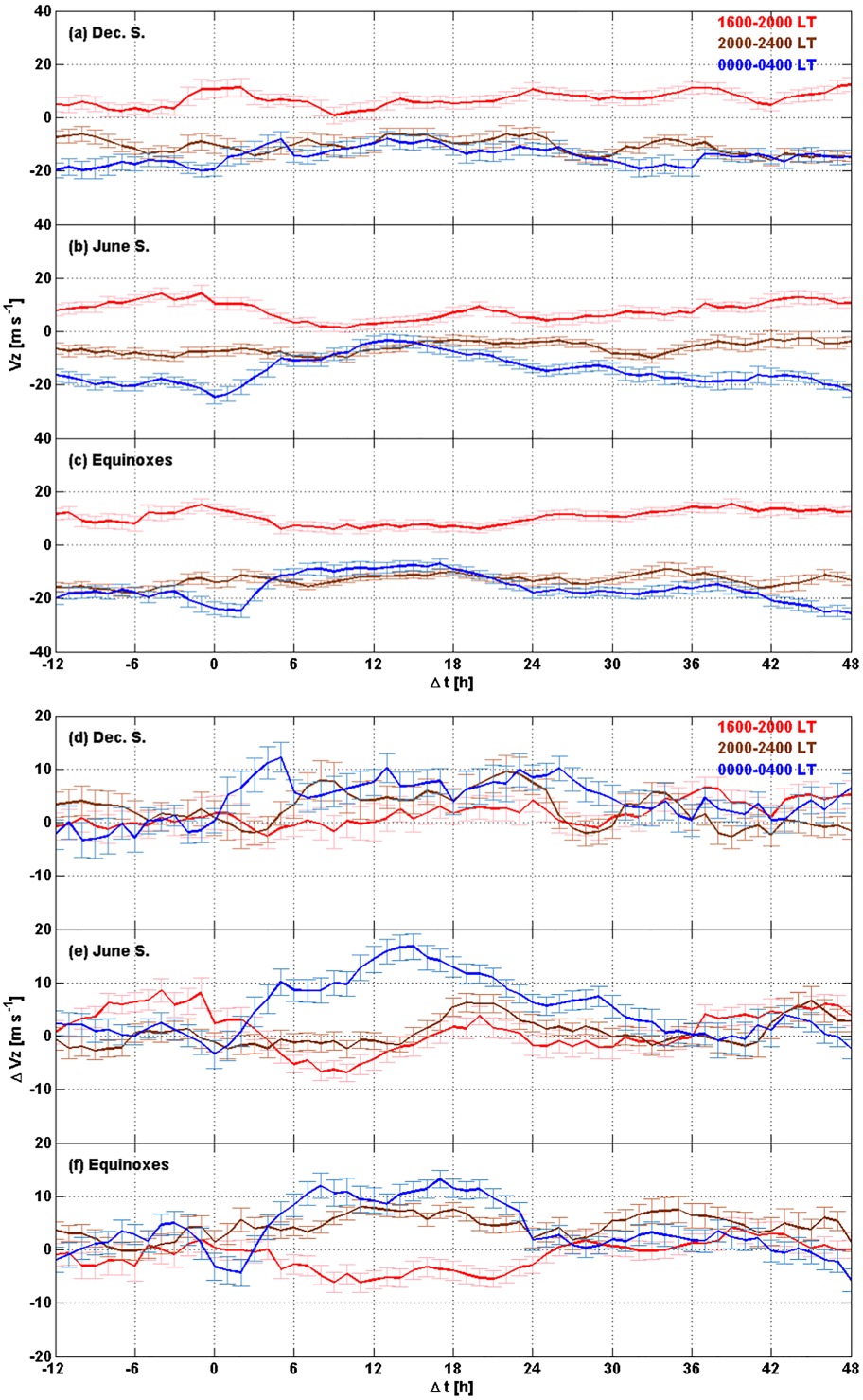

Figure 3. Same as Figure 2 but for the ion vertical drift.

An interesting question about the postmidnight EPDs is whether they are newly generated during postmidnight hours or they are the heritages (fossil EPDs) from earlier local time. We tried to answer this question by comparing if the observed EPDs had already been observed in previous orbits. Figure 4 presents the examples of EPDs which were continuously observed at midnight and predawn during the storm on 13 October 2000. The persistent EPDs are detected near South America during five consecutive satellite passes; the time

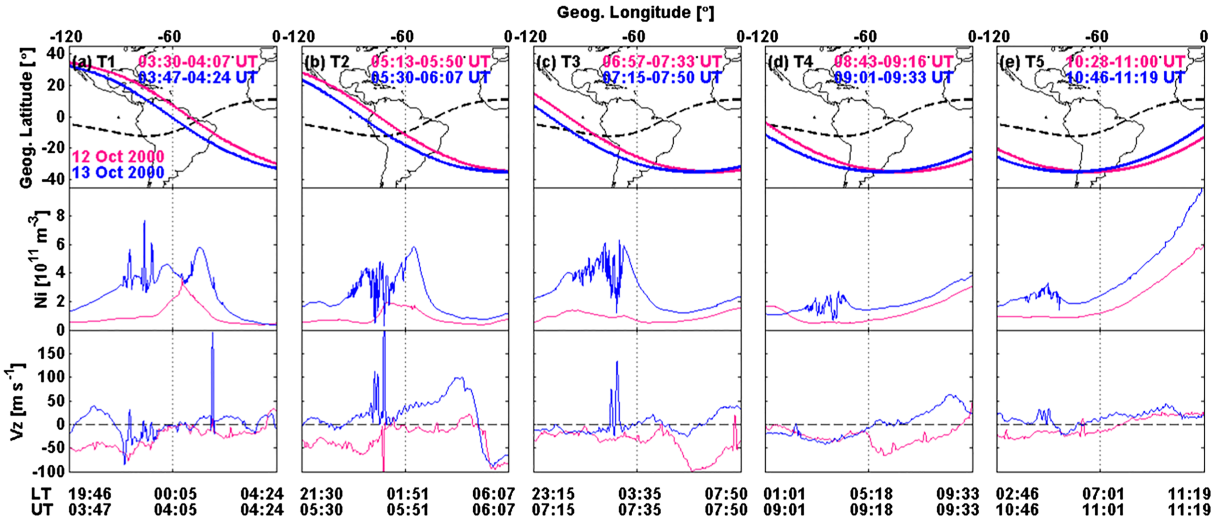

Figure 4. Five consecutive orbits over South America during the recovery phase of 13 October 2000 storm (blue curve) and similar passes at same UT on 12 October 2000 (magenta curve), the UT of each orbit arch is specified as "T1"–"T5" as denoted in Figure 1a.

segments of each pass are labeled as "T1"–"T5" which are within the first recovery phase, as shadowed in Figure 1a. In comparison, measurements on the day before (12 October 2000) are also presented as the reference and colored in magenta. The EPD firstly appears at T1 before 2400 LT, meanwhile, the V_z is enhanced and remain upward to "T3" compared to the downward V_z on 12 October. Considering that the T1 is about 5 hr later after the southward turning of IMF B_z which is sufficient for the development of the DDEF. The DDEF induced enhanced upward V_z could be the main factor to favor the EPDs occurrence. The EPD continuously survived to T3 and "T4" when the background *Ni* is reduced, so as the depletion amplitudes, meanwhile, the local time had moved into predawn sector. The EPD finally decayed near dawn at T5. Thus, predawn EPDs at T3/T4/T5 could be recognized as the fossil Midnight EPDs at T1 and "T2." Due to the fact that the satellite fled at opposite hemisphere when South America is in postsunset compare to that in predawn, it is not possible to determine whether the predawn EPDs could be witnessed earlier in postsunset.

We further check the fossil feature of predawn EPDs from a statistical sense. Several steps are made to find the predawn EPDs whose signatures can be traced back before or around midnight. The epoch time is firstly divided into three segments depend on whether more predawn EPDs are detected, 3–24 hr, referred as storm time (ST) when the predawn EPDs occurrence is enhanced and the other time segments (−48–2 hr, referred as pre-ST; 25–72 hr, referred as post-ST). The predawn EPDs are subsequently sorted out and their longitudinal coverages are recorded. For each predawn EPDs event, we look back to three previous orbits when the recorded longitudinal coverage was in earlier local time. If the EPDs were still detected, it is recognized as fossil EPDs which is traceable through earlier local time to predawn. For each epoch time segment, the total number of satellite pass is also recorded. The original number satellite pass with predawn EPDs is divided by the total number of satellite pass and subsequently normalized to a proper number by multiplying a constant coefficient. Here we set the proper number of predawn EPDs during 6–24 hr of equinoxes as 100. We note that the total pass numbers with predawn EPDs detected in each category could be regard as the relative occurrence rate when it is divided by 100, and the occurrence rate of predawn EPDs during 3–24 hr in equinoxes is manually set as 100%.

The statistical result is shown in Table 1. As expected, the total number of satellite pass with predawn EPDs detected during ST is significantly increased from that during pre-ST and post-ST. The percentage of traceable predawn EPDs during pre-ST and post-ST are comparable for all three seasons which is around 46% for December solstice, 40% for June solstice, and 31% for equinoxes. When it comes to ST, percentage of passes with traceable predawn EPDs is 52% for December solstice, 54% for June solstice, and 60% for December solstice, which show a persistent increase for all three seasons from that of pre-ST and post-ST.

Table 1
Normalized Number of Predawn EPDs When the Occurrence Is Enhanced (6–24 hr, Colored in Orange) or Not Enhanced (−48–5 and 25–72 hr, colored in blue) in the SEA

Normalized pass numbers with predawn EPDs	−48–2 hr (Pre-ST)		3–24 hr (ST)		25–72 hr (Post-ST)	
	Total	Traceable	Total	Traceable	Total	Traceable
Dec. S.	30	14, 47%	95	49, 52%	25	11, 46%
June S.	35	14, 41%	78	42, 54%	27	11, 40%
Equinoxes	17	5, 31%	100	60, 60%	34	11, 31%

Note. The numbers/percentages of Pre-dawn EPDs which could be traced back at earlier local time is listed in the second column of each category, respectively.

The largest amplitude of this increasing occurs during equinoxes which neatly reaches to 30%, and only a 5% increase occurs during December solstice.

3.2. Longitudinal Variations

Due to the inadequate amount of data set, the longitudinal distinguished SEA on the storm period EPDs occurrence is not operable. As we may notice in section 5, the EPDs occurrence is generally enhanced for predawn sector and suppressed for postsunset and midnight, which is the major characteristic of EPDs during geomagnetic storms. This climatology is highly possible attributed to the DDEF induced different V_z perturbations regarding three local time sectors. Thus, we turn to the *Kp*, which show a positive correlation with Joule heating in the high-latitude region (Foster et al., 1983) which further influence the global wind circulation to drive the DDEF, as the indicator of geomagnetic disturbances.

Figure 5 firstly shows the global distribution of EPDs occurrence rate during geomagnetic quiet periods ($Kp < 3$), as the references. With the same sorting process, the V_z is also presented in different longitudes and its magnitude is quantified by the right *Y* axis. The seasonal/longitudinal variation of the EPDs occurrence rate is in consist with previous studies (e.g., Burke, Huang, et al., 2004; Su et al., 2006, 2008; Stolle et al., 2008; Xiong et al., 2010; Wan et al., 2018). For postsunset sector, V_z is also well correlated with the occurrence of the EPDs. Nevertheless, the correlations between EPDs occurrence and V_z can be barely found for predawn sector in a manner of their longitudinal variations.

Figure 6 is plotted in the same way as Figure 5 but for the occurrence of EPD when $Kp \geq 3$. We see that the longitudinal dependence of the EPDs occurrence is in the same pattern to that during geomagnetic quiet periods (Figure 5). However, for postsunset sector, the occurrence rates are lower than that during geomagnetic quiet periods at almost all the longitudes; for midnight sector, the occurrence rate is also reduced at most areas, except at the eastern Pacific during December solstice and South America to Atlantic during June solstice; for predawn sector, the occurrence rate is generally higher than that of geomagnetic quiet periods. Still, the V_z varies in the same pattern but with relatively larger values compared to that during geomagnetic quiet periods.

To visualize the consequences of geomagnetic disturbances on the EPDs occurrence and the V_z, we subtract the statistic results of periods of $Kp < 3$ from that of $Kp \geq 3$. The residual maps are given in Figure 7, as labeled as Residual occurrence rate and ΔV_z. For most EPDs prevailing longitudes at postsunset, the residual occurrence rate is negative (e.g., South America to Atlantic of December solstice; Africa and mid-Pacific of June solstice; South America to Southeast Asia of equinoxes). Meanwhile, enhanced occurrence rate does exist at some longitudes (e.g., middle east Pacific of December solstice; east Pacific to Atlantic of June solstice) where the EPDs occurrence does not prevails. The longitudinal variations of V_z correlated well with the EPDs occurrence for two solstices (Figures 7a and 7d). However, the positive ΔV_z do exist at postsunset when the EPDs occurrence is universally suppressed (Figure 7g). For midnight sector, the enhanced EPDs occurrence appears in more and wider regions that are still confined in longitudes where the EPDs is not prevailing. At predawn sector, most of the longitudes experience the enhanced occurrence of EPDs which suggested the continued expansion of regions with enhanced occurrence from midnight. However, for both midnight and predawn sectors, the ΔV_z is positive at all the longitudes, and the correlations between V_z with EPDs occurrence is not as prominent as that of postsunset.

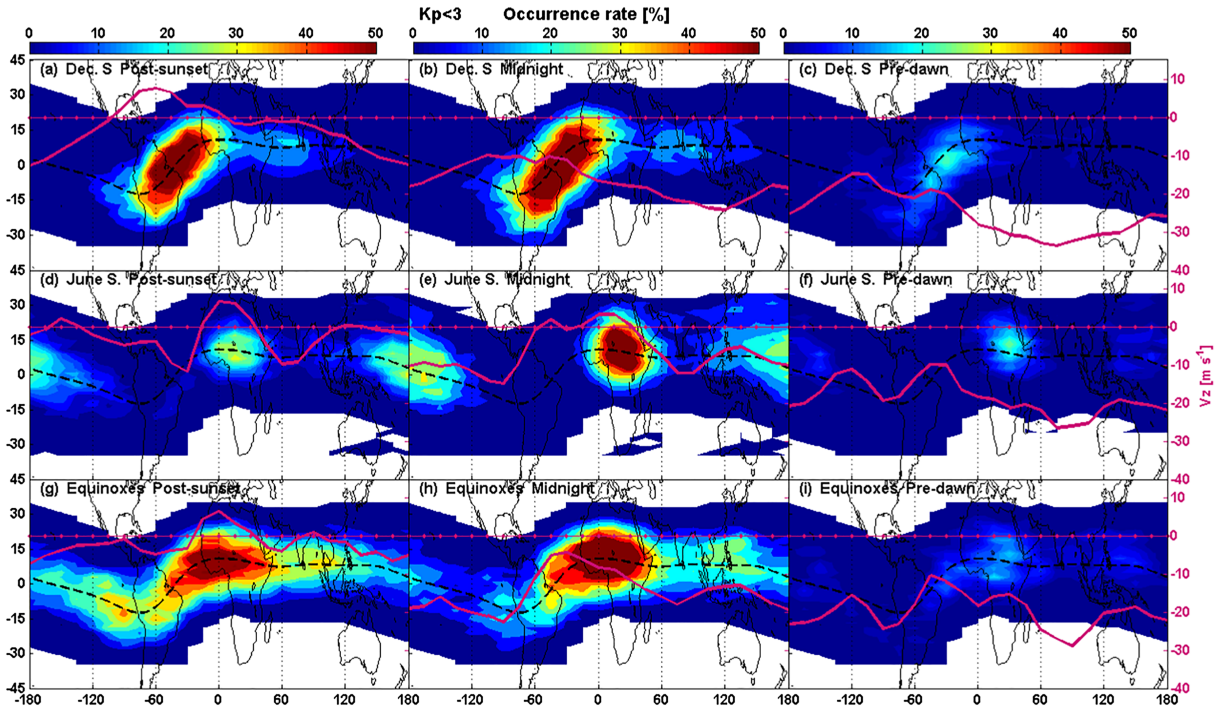

Figure 5. Global contours of EPDs occurrence and the plots of the plasma vertical drift (colored in dark pink and quantified by *Y* axis at the right side) under the condition when the $Kp < 3$. The black dash line is the dip equator.

4. Discussion

4.1. SEA on the EPDs Occurrence and Plasma Vertical Drift

EPDs occurrence exhibit a temporary enhancement for the postsunset and midnight sectors during all three seasons from $\Delta t = 00$ hr (red and blue curves in Figures 2a–2c). This enhancement is also recurrence in the residual occurrence plotting for December solstice and June solstice (Figures 2d and 2e) after removing the quiet time reference. Correspondingly at postsunset sector, similar signals on the epoch time variation of V_z are also witnessed (red curves in Figures 3a–3c). The correlations between postsunset/Midnight EPDs occurrence with postsunset V_z near $\Delta t = 00$ hr have been identified for all three seasons. Since storm commencement is frequently accompanied by the southward turning of IMF B_z (Yokoyama & Kamide, 1997), we suggest that the associated PPEF which enlarges the upward vertical plasma drift velocity near sunset (PRE) is the cause of the promotion of the postsunset EPDs occurrence. Theoretically, the PPEF is westward during nighttime (Fejer et al., 2008b) which suppress the growth rate of the EPDs which supposed to appear at midnight and predawn, at ROCSAT-1 altitude. However, this inhibited signature is not captured at either midnight or predawn in our results. Stolle et al. (2008) found a 2–3 hr lag for the ESF occurrence (captured by CHAMP at about 400 km) to respond to PRE. Longer responding time is promised when EPDs are detected at altitudes above 600 km where ROCSAT-1 flew. Thus, the midnight EPDs as detected by ROCSAT-1 should be mainly generated near postsunset when the PRE is still effective (V_z at postsunset), which further leads to a nearly synchronized epoch time variation of midnight EPDs to that of postsunset. Since the occurrence of predawn EPDs is normally (during geomagnetic quiet periods) much rarer compared to that of postsunset, the inhibition signal might not be easy to capture especially under the circumstance that the PPEF is short lived.

The short-duration enhancement of EPDs occurrence at postsunset/midnight is followed by an inhibition which could last for longer than 1 day. The long-lasting inhibition signal is more prominent at postsunset than that at midnight and for equinoxes than that for the other two seasons. In the meantime, the EPDs occurrence at predawn (blue curves in Figures 2a–2c) starts to increase near $\Delta t = 00$ hr and reach to the peaks around 6–9 hr. So as seen in the residual plotting (blue curves in Figures 2d–2f), the enhanced occurrence could last at least till 18 hr. Correspondingly, V_z at postsunset (Figures 3a–3c) decreases for about 9 hr

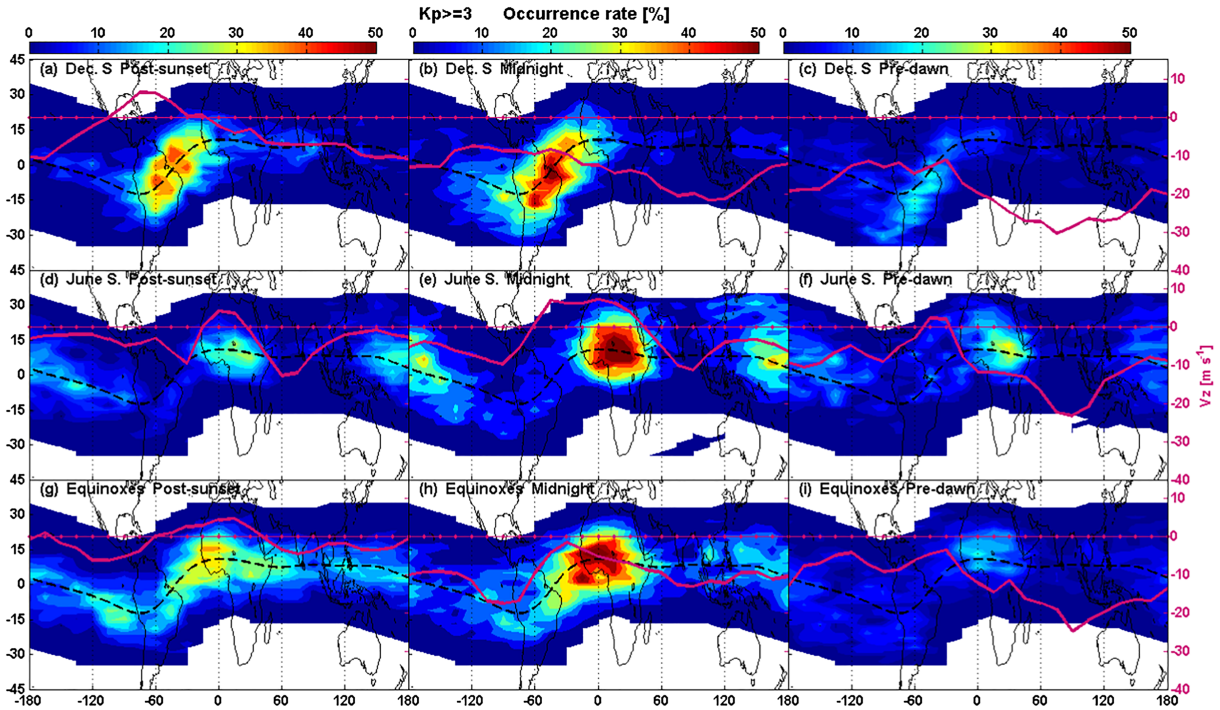

Figure 6. Same as Figure 5 but under the condition when $Kp \geq 3$.

for all three seasons; after removing the quiet time occurrence pattern, the negative postsunset ΔV_z dominates during 03–18 and 03–30 hr in respect to June solstice and equinoxes. V_z at midnight is ambiguity while V_z at predawn exhibit clear enhancement shortly after epoch 0 hr. The residual plotting shows the positive ΔV_z at predawn throughout 03–36 hr for all three seasons, and the ΔV_z at Midnight only tends to share the positive signals as that at predawn for equinoxes. The long-lasting DDEF, which forms 3–4 hr after energy input at high-latitude during geomagnetic disturbed periods, should be the fundamental mechanism to determine the negative/positive ΔV_z and explains the long-duration promotion/suppression of EPDs occurrence at postsunset/predawn. As we noted before, the DDEF changes its polarization near 2200 LT (Fejer et al., 2008b), thus, the polarization of disturbed V_z at Midnight (2000–2400 LT) could not be clearly determined.

The general climatology of EPDs occurrence and associated V_z agree well with our understanding of the disturbed equatorial electric fields (e.g., Abdu, 2012; Abdu et al., 2012; Fejer et al., 2008b). The enhanced upward V_z at postsunset serves as the key factor to contribute to the well-known R-T instabilities growth rate and facilitate the generation of the postsunset/midnight EPDs.

Situation changes for the EPDs occurrence at predawn as the absolute value of V_z is still statistically negative which is not a favorable condition on the growth of the R-T instabilities. The question raised to our mind is how the geomagnetic storms induced weaken of downward V_z benefit the EPDs occurrence at predawn hours. Whether the additional predawn EPDs are freshly generated from the bottom side ionosphere or the prolonged EPDs which has already propagated to the topside and survived till predawn? In other words, is it in the same way that the weaken of downward V_z contribute to the predawn EPDs occurrence as to that of enhancing of upward V_z contribute to postsunset EPDs? To resolve the question, we trace the predawn EPDs back to previous satellite orbits to check whether they already exist at earlier local times.

Seasonal variation is firstly identified during pre-ST and post-ST that about 46%, 40%, or 31% of passes with traceable pre-dawn EPDs could be traced at earlier local time for December solstice/June solstice/equinoxes (Table 1), which could be recognized as the normal pattern. However, compared to that during pre-ST and post-ST, enhancements of the percentage of pass with traceable predawn EPDs occur during ST for all three seasons. The enhancement indicates that the addition predawn during ST is more related to old

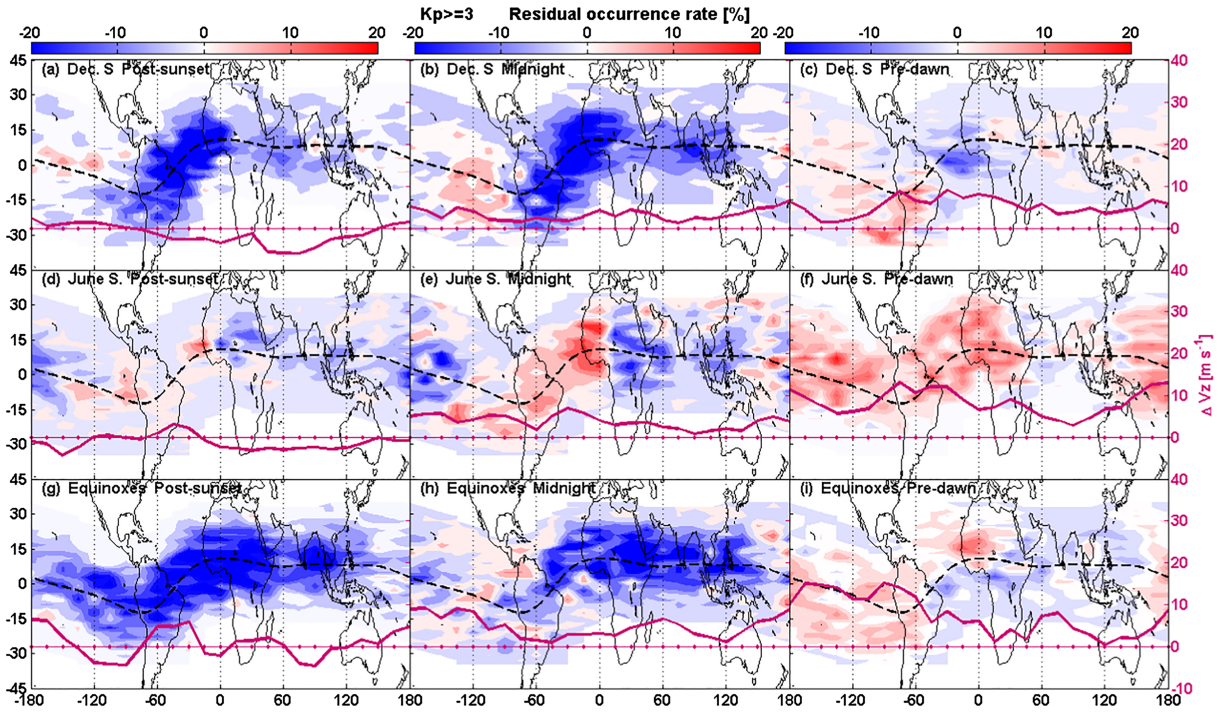

Figure 7. The residual occurrence rate of EPDs and the residual plasma vertical drift during periods of $Kp \geq 3$.

EPDs which already exist at earlier local time at the same altitude, which could be regarded as the fossil EPDs. Thus, we suggest that the geomagnetic disturbances benefit the occurrence predawn EPDs mainly by maintaining the old ones instead of by initiating fresh EPDs. Besides, the amplitude of the increasing is largest during Equinoxes which reaches to 30% while it is about 5% and 13% for December solstice and June solstice. This seasonal preference might be the consequence of the longitudinal variation of storm-induced predawn EPDs and the PRE. We note that the storm-induced additional predawn EPDs has a longitudinal preference at Pacific but without seasonal preference (Figures 7c–7i), while the background PRE strength at Pacific is strongest during Equinoxes and weakest during December solstice (Fejer et al., 2008a). The different seasonal behavior between predawn EPDs occurrence with PRE strength over Pacific might be the reason why equinoxes exhibit largest increase of percentage of passes with traceable predawn EPDs.

4.2. Longitudinal Variations

The inhibition/promotion of geomagnetic storm induced EPDs occurrence shows also longitudinal dependence, in addition to the seasonal and local time variations. Previous works had revealed an interesting phenomenon, that is, the EPDs during geomagnetic disturbed period are triggered during EPDs seasons and suppressed during non-EPDs seasons (Aarons et al., 1991; Rastogi et al., 1981; Becker-Guedes et al., 2004; Sun et al., 2012). For example, Sun et al. (2012) provided statistical evidence that the postsunset EPDs occurrence is significantly suppressed in the months (September–March) that normally have high occurrence and triggered in low occurrence months (April–August) at Brazilian sector. However, as far as we know, all these works are based on ground observations and the spatial coverage is confined within South America. From a global view, our observations confirmed this point and further reveal that the EPDs occurrence at postsunset tends to be suppressed at longitudes where EPDs prevail and promoted at longitudes where EPDs do not prevails. The exception lies in middle Asia during June solstice when the EPDs occurrence is supposed to be increased under geomagnetic disturbed condition, but as shown in our Figure 7d, the EPDs occurrence is suppressed. Still, this longitude determined suppression/promotion of postsunset EPDs occurrence is related with the residual V_z (e.g., higher ΔV_z meets enhanced occurrence at Pacific during December solstice; Figure 7a). Nevertheless, this pattern cannot be applied for the EPDs occurrence at predawn sector.

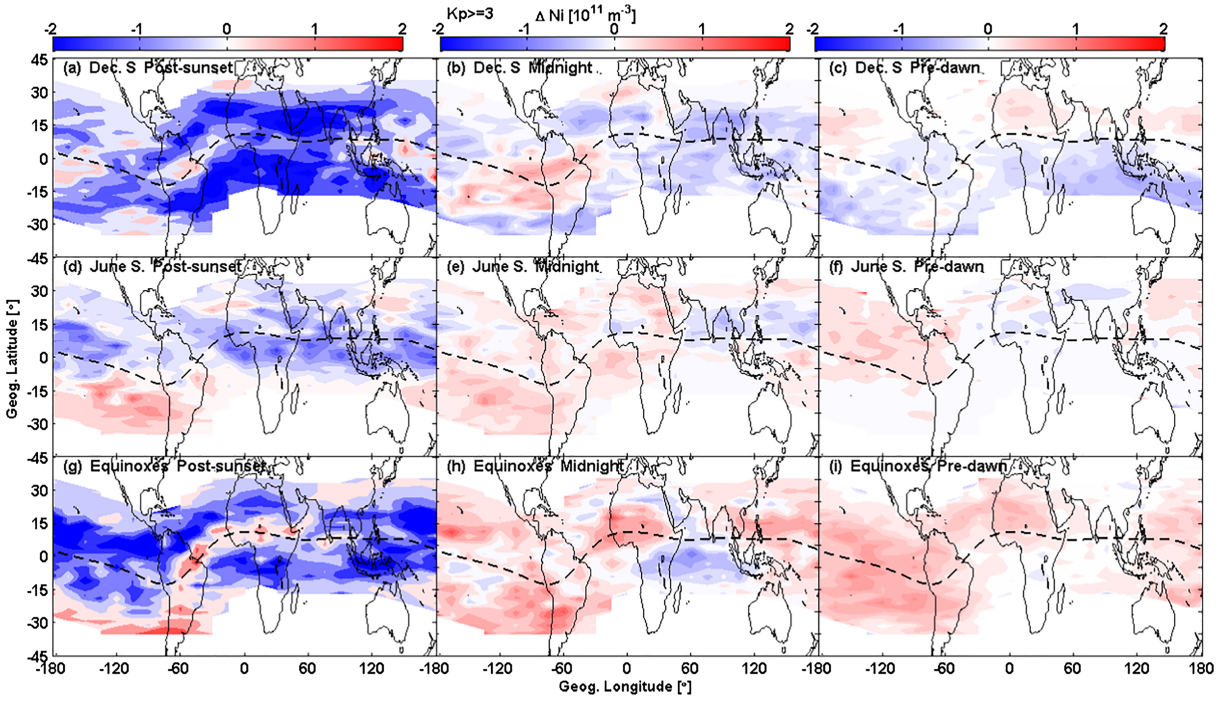

Figure 8. Same as Figure 7 but for the background ion density.

Residual EPDs occurrence at Midnight basically shares the same pattern with that at the postsunset hours. However, longitudes with enhanced occurrence are expanded (e.g., South America during equinoxes in Figure 6h) and the enhancement is also more prominent compared to that of postsunset hours. The intensity and the longitude coverage of the occurrence enhancement are continued to be enhanced at predawn. The trends of the increased intensity as well as spatial coverage of the EPDs occurrence promotion from postsunset to predawn are related to the positive ΔV_z at midnight and predawn. However, the ΔV_z is not enough to explain the longitudinal variation of the residual occurrence, as we can witness that the ΔV_z failed to match the residual occurrence rate neither on the intensity (e.g., Pacific verse Atlantic during equinoxes; Figure 7i) nor on the polarization (e.g., Atlantic during December solstice; Figure 7c). As illustrated in the last paragraph, the predawn EPDs partly heritage from the EPDs of midnight/postsunset, and the geomagnetic storms strengthen the process. The suppression of EPDs occurrence at midnight/postsunset would consequently lead to the reduced developed/developing EPDs which are supposed to survive till predawn.

Moreover, we note that the EPDs prefer to occur at the longitudes from Pacific to South America regardless of seasons for midnight and predawn (Figure 7). This longitudinal preference brings some clues concerning the impact from the energetic particles. It was found that kilo-electron-volt energetic electrons from the inner radiation belt can penetrate to the ionospheric F region at low latitudes outside the SAA region (Suvorova et al., 2013, 2014). During periods when geomagnetic field is disturbed, the energetic electron (quasi-trapped kind) fluxes are sporadically enhanced near the equator, at longitudes beyond SAA, for several hours. Along with the prolonged eastward azimuth drift, these electrons deposit most energy near the mirror points at latitudes 10°–30° off the dip equator due to collisions with atmospheric neutral species in the topside ionosphere, cause a noticeable enhancement in the total electron content and topside electron/ion density (Suvorova et al., 2013, 2014, 2016).

Figure 8 shows the contour of the ion density perturbations (ΔNi), as plotted in the same way as that of the residual EPDs occurrence rate, during geomagnetic disturbed periods when $Kp \geq 3$. For postsunset, the ΔNi at most areas of the world is negative which could be mainly attributed to the downward disturbed vertical plasma drift. The Ni enhancements at region of Pacific to South America in the Southern Hemisphere (SAA and westward) exhibit differently. The same pattern of Ni enhancements is also noticeable at midnight and predawn, especially during equinoxes. Coincidently, energetic electrons, the flux of which could be

significantly intensified during geomagnetic storms, are also preferred to be detected at longitudes from Pacific to South America (Figure 2 in Suvorova et al., 2013), at a local time near midnight (Suvorova, 2017). These coincidences bring insights into the nighttime ionization resulted in the ionospheric positive storm, which further benefits the occurrence of EPDs especially at midnight and after.

Although the ion density measured by the ROCSAT-1 satellite is at altitudes above the *F* region, plasma density at altitudes near the *F* peak should be resulted from either direct ionization or diffusion from the ionized topside ionosphere (Suvorova et al., 2016). Besides, the EPDs are found to stop rising when the magnetic flux-tube integrated ion mass density inside EPD equals to that of the surrounding background ionosphere (Krall et al., 2010; Mendillo et al., 2005). Therefore, we suggest that the higher background density at the *F* region or topside ionosphere benefit the development of the EPDs in two aspects: (1) by increasing the growth of EPD along flux tube, due to the enhanced flux tube-integrated *F* region conductivity and (2) by keeping the developed EPD rising upward or staying stationary as the fossilized one. Both scenarios resulted in that the EPDs could survive longer and higher, thus, leading to a more frequent appearance at the topside ionosphere, especially at late night (midnight/predawn) when the background plasma density normally keeps in a low level and gets considerable enhancement during disturbed periods.

5. Summary

Based on in situ plasma density measurements of ROCSAT-1 satellite, during 181 geomagnetic storms happened from July 1999 to June 2004, the season/LT distinguished EPDs occurrence are analyzed and presented in this study. The main findings are summarized as below:

1. The occurrence at postsunset and midnight is shortly enhanced near storm onset which should be related to the PPEF that strengthens the PRE; A long-last suppression dominates afterward which should be related to the DDEF that weakens the PRE. The occurrence at predawn gradual increase after storm onset and reach its maximum at 6–9 hr and decays after 18 hr.
2. Most of the EPDs at predawn are the heritages from that at earlier local time (mainly during midnight). We suggest that the geomagnetic disturbances benefit predawn EPDs occurrence mainly by maintaining the existing EPDs at same altitude from earlier local time rather than facilitating fresh generated EPDs.
3. For postsunset and midnight, the EPDs occurrence generally tends to be suppressed (promoted) at longitudes where the EPDs normally prevails (does not prevails), except that at mid-Asia during June solstice. The longitudinal variation of plasma vertical drift near sunset is account for this pattern. For predawn sector, the EPDs occurrence tends to be promoted for most longitudes, detailed longitudinal determination of enhanced/suppressed occurrence show less correlation with plasma vertical drift.
4. At the Pacific-Atlantic region, the EPDs occurrence exhibits a persistent enhancement at midnight and predawn for all seasons. Correspondingly, the same enhancement on the background ion density as well as energetic electron flux (Figure 2 of Suvorova et al., 2013) are also witnessed, which indicates a close link with additional nighttime ionization induced by the energetic electrons from inner radiation belt. We suggest that the background plasma density enhancement at topside *F* region benefits the EPDs occurrence, in a form concerning the development of the developing EPDs and the maintenance of fossil EPDs.

Acknowledgments
The authors thank NASA's OMNIweb (https://omniweb.gsfc.nasa.gov/ow_min.html) for providing the solar wind, IMF data, and the geomagnetic indices. The ROCSAT-1 data sets were provided by the National Central University, which can be downloaded from http://sdbweb.ss.ncu.edu.tw/ipei_download.html website. The work of X. W. and H. W. is supported by National Natural Science Foundation of China (41674153, 41521063, and 41431073).

References

Aarons, J. (1991). The role of the ring current in the generation or inhibition of equatorial F layer irregularities during magnetic storms. *Radio Science*, *26*(4), 1131–1149. https://doi.org/10.1029/91RS00473

Abdu, M. A. (2012). Equatorial spread *F*/plasma bubble irregularities under storm time disturbance electric fields. *Journal of Atmospheric and Solar - Terrestrial Physics*, *75–76*, 44–56.

Abdu, M. A., Batista, I. S., Bertoni, F., Reinisch, B. W., Kherani, E. A., & Sobral, J. H. A. (2012). Equatorial ionosphere responses to two magnetic storms of moderate intensity from conjugate point observations in Brazil. *Journal of Geophysical Research*, *117*, A05321. https://doi.org/10.1029/2011JA017174

Abdu, M. A., De Paula, E. R., Batista, I. S., Reinisch, B. W., Matsuoka, M. T., Camargo, P. O., et al. (2008). Abnormal evening vertical plasma drift and effects on ESF and EIA over Brazil-South Atlantic sector during the 30 October 2003 superstorm. *Journal of Geophysical Research*, *113*, A07313. https://doi.org/10.1029/2007JA012844

Batista, I. S., Abdu, M. A., Souza, J. R., Bertoni, F., Matsuoka, M. T., Camargo, P. O., & Bailey, G. J. (2006). Unusual early morning development of the equatorial anomaly in the Brazilian sector during the Halloween magnetic storm. *Journal of Geophysical Research*, *111*, A05307. https://doi.org/10.1029/2005JA011428

Blanc, M., & Richmond, A. (1980). The ionospheric disturbance dynamo. *Journal of Geophysical Research*, *85*, 1669–1686. https://doi.org/10.1029/JA085iA04p01669

Becker-Guedes, F., Sahai, Y., Fagundes, P. R., Lima, W. L. C., Pillat, V. G., Abalde, J.R., & Bittencourt, J. A. (2004). Geomagnetic storm and equatorial spread-F. *Annales Geophysicae*, *22*, 3231–3239. https://doi.org/10.5194/angeo-22-3231-2004

Burke, W. J., Gentile, L. C., Huang, C. Y., Valladares, C. E., & Su, S. Y. (2004). Longitudinal variability of equatorial plasma bubbles observed by DMSP and ROCSAT-1. *Journal of Geophysical Research*, *109*, A12301. https://doi.org/10.1029/2004JA010583

Burke, W. J., Huang, C. Y., Gentile, L. C., & Bauer, L. (2004). Seasonal-longitudinal variability of equatorial plasma bubble occurrence. *Annales Geophysicae*, *22*(9), 3089–3098. https://doi.org/10.5194/angeo-22-3089-2004

Carter, B. A., Yizengaw, E., Pradipta, R., Retterer, J. M., Groves, K., Valladares, C., et al. (2016). Global equatorial plasma bubble occurrence during the 2015 St. Patrick's Day storm. *Journal of Geophysical Research: Space Physics*, *121*, 894–905. https://doi.org/10.1002/2015JA022194

Carter, B. A., Zhang, K., Norman, R., Kumar, V. V., & Kumar, S. (2013). On the occurrence of equatorial *F*-region irregularities during solar minimum using radio occultation measurements. *Journal of Geophysical Research: Space Physics*, *118*, 892–904. https://doi.org/10.1002/jgra.50089

Dao, T., Otsuka, Y., Shiokawa, K., Nishioka, M., Yamamoto, M., Buhari, S. M., et al. (2017). Coordinated observations of postmidnight irregularities and thermospheric neutral winds and temperatures at low latitudes. *Journal of Geophysical Research: Space Physics*, *122*, 7504–7518. https://doi.org/10.1002/2017JA024048

Fejer, B. G., Jensen, J. W., & Su, S.-Y. (2008a). Quiet time equatorial *F* region vertical plasma drift model derived from ROCSAT-1 observations. *Journal of Geophysical Research*, *113*, A05304. https://doi.org/10.1029/2007JA012801

Fejer, B. G., Jensen, J. W., & Su, S.-Y. (2008b). Seasonal and longitudinal dependence of equatorial disturbance vertical plasma drifts. *Geophysical Research Letters*, *35*, L20106. https://doi.org/10.1029/2008GL035584

Foster, J. C., St.-Maurice, J.-P., & Abreu, V. J. (1983). Joule heating at high latitudes. *Journal of Geophysical Research*, *88*(A6), 4885–4897. https://doi.org/10.1029/JA088iA06p04885

Hairston, M. R., Coley, W. R., & Stoneback, R. (2013). Vertical and meridional equatorial ion flows observed by CINDI during the 26 September 2011 storm. *Journal of Geophysical Research: Space Physics*, *118*, 5230–5243. https://doi.org/10.1002/jgra.50411

Horvath, I., & Lovell, B. C. (2010). Traveling ionospheric disturbances and their relations to storm-enhanced density features and plasma density irregularities in the local evening and nighttime hours of the Halloween superstorms of 29–31 October 2003. *Journal of Geophysical Research*, *115*, A09327. https://doi.org/10.1029/2009JA015125

Huba, J. D., & Krall, J. (2013). Impact of meridional winds on equatorial spread *F*: Revisited. *Geophysical Research Letters*, *40*, 1268–1272. https://doi.org/10.1002/grl.50292

Jian, L., Russell, C. T., Luhmann, J. G., & Skoug, R. M. (2006). Properties of interplanetary coronal mass ejections at one AU during 1995–2004. *Solar Physics*, *239*, 393.

Kelley, M. C., Fejer, B. G., & Gonzales, C. A. (1979). An explanation for anomalous equatorial ionospheric electric field associated with a northward turning of the interplanetary magnetic field. *Geophysical Research Letters*, *6*, 301.

Kelly, M. C. (2009). *The Earth's ionosphere: Plasma physics and electrodynamics* (2nd ed.). Boston: Academic Press.

Krall, J., Huba, J. D., Joyce, G., & Hei, M. (2013). Simulation of the seeding of equatorial spread *F* by circular gravity waves. *Geophysical Research Letters*, *40*, 1–5. https://doi.org/10.1029/2012GL054022

Krall, J., Huba, J. D., Joyce, G., & Zalesak, S. T. (2009). Three-dimensional simulation of equatorial spread-*F* with meridional wind effects. *Annales de Geophysique*, *27*, 1821–1830. https://doi.org/10.5194/angeo-27-1821-2009

Krall, J., Huba, J. D., Ossakow, S. L., & Joyce, G. (2010). Why do equatorial ionospheric bubbles stop rising? *Geophysical Research Letters*, *37*, L09105. https://doi.org/10.1029/2010GL043128

Krall, J., Huba, J. D., Ossakow, S. L., Joyce, G., Makela, J. J., Miller, E. S., & Kelley, M. C. (2011). Modeling of equatorial plasma bubbles triggered by non-equatorial traveling ionospheric disturbances. *Geophysical Research Letters*, *38*, L08103. https://doi.org/10.1029/2011GL046890

Lei, J., Wang, W., Burns, A. G., Yue, X., Dou, X., Luan, X., et al. (2014). New aspects of the ionospheric response to the October 2003 superstorms from multiple-satellite observations. *Journal of Geophysical Research: Space Physics*, *119*, 2298–2317. https://doi.org/10.1002/2013JA019575

Li, G., Ning, B., Hu, L., Liu, L., Yue, X., Wan, W., et al. (2010). Longitudinal development of low-latitude ionospheric irregularities during the geomagnetic storms of July 2004. *Journal of Geophysical Research*, *115*, A04304. https://doi.org/10.1029/2009JA014830

Maruyama, T., Saito, S., Kawamura, M., Nozaki, K., Krall, J., & Huba, J. D. (2009). Equinoctial asymmetry of a low-latitude ionosphere-thermosphere system and equatorial irregularities: Evidence for meridional wind control. *Annales de Geophysique*, *27*, 2027–2034. https://doi.org/10.5194/angeo-27-2027-2009

McClure, J. P., Singh, S., Bamgboye, D. K., Johnson, F. S., & Kil, H. (1998). Occurrence of equatorial *F* region irregularities: Evidence for tropospheric seeding. *Journal of Geophysical Research*, *103*(A12), 29119–29135. https://doi.org/10.1029/98JA02749

Mendillo, M., Zesta, E., Shodham, S., Sultan, P. J., Doe, R., Sahai, Y., & Baumgardner, J. (2005). Observations and modeling of the coupled latitude-altitude patterns of equatorial plasma depletions. *Journal of Geophysical Research*, *110*, A09303. https://doi.org/10.1029/2005JA011157

Murphy, J. A., & Heelis, R. A. (1986). Implications of the relationship between electromagnetic drift components at mid and low latitudes. *Planetary and Space Science*, *34*(7), 645–652.

Rastogi, R. G., Mullen, J. P., & MacKenzie, E. (1981). Effect of geomagnetic activity on equatorial radio VHF scintillations and spread F. *Journal of Geophysical Research*, *86*(A5), 3661–3664. https://doi.org/10.1029/JA086iA05p03661

Senior, C., & Blanc, M. (1984). On the control of magnetospheric convection by the spatial distribution of ionospheric conductivity. *Journal of Geophysical Research*, *89*, 261.

Smith, J. M., & Heelis, R. A. (2018). Plasma dynamics associated with equatorial ionospheric irregularities. *Geophysical Research Letters*, *45*. https://doi.org/10.1029/2018GL078560

Stolle, C., Lühr, H., & Fejer, B. G. (2008). Relation between the occurrence rate of ESF and the equatorial vertical plasma drift velocity at sunset derived from global observations. *Annales Geophysicae*, *26*(12), 3979–3988. https://doi.org/10.5194/angeo-26-3979-2008

Su, S.-Y., Chao, C. K., & Liu, C. H. (2008). On monthly/seasonal/longitudinal variations of equatorial irregularity occurrences and their relationship with the postsunset vertical drift velocities. *Journal of Geophysical Research*, *113*, A05307. https://doi.org/10.1029/2007JA012809

Su, S.-Y., Liu, C. H., Ho, H. H., & Chao, C. K. (2006). Distribution characteristics of topside ionospheric density irregularities: Equatorial versus midlatitude regions. *Journal of Geophysical Research*, *111*, A06305. https://doi.org/10.1029/2005JA011330

Sultan, P. J. (1996). Linear theory and modeling of the Rayleigh-Taylor instability leading to the occurrence of equatorial spread *F*. *Journal of Geophysical Research*, *101*, 26,875–26,891.

Sun, Y. Y., Liu, J. Y., & Lin, C. H. (2012). A statistical study of low latitude *F* region irregularities at Brazilian longitudinal sector response to geomagnetic storms during post-sunset hours in solar cycle 23. *Journal of Geophysical Research*, *117*, A03333. https://doi.org/10.1029/2011JA017419

Suvorova, A. V. (2017). Flux enhancements of >30 keV electrons at low drift shells L < 1.2 during last solar cycles. *Journal of Geophysical Research: Space Physics*, *122*, 12,274–12,287. https://doi.org/10.1002/2017JA024556

Suvorova, A. V., Dmitriev, A. V., Tsai, L.-C., Kunitsyn, V. E., Andreeva, E. S., Nesterov, I. A., & Lazutin, L. L. (2013). TEC evidence for near-equatorial energy deposition by 30 keV electrons in the topside ionosphere. *Journal of Geophysical Research: Space Physics*, *118*, 4672–4695. https://doi.org/10.1002/jgra.50439

Suvorova, A. V., Huang, C.-M., Dmitriev, A. V., Kunitsyn, V. E., Andreeva, E. S., Nesterov, I. A., et al. (2016). Effects of ionizing energetic electrons and plasma transport in the ionosphere during the initial phase of the December 2006 magnetic storm. *Journal of Geophysical Research: Space Physics*, *121*, 5880–5896. https://doi.org/10.1002/2016JA022622

Suvorova, A. V., Huang, C.-M., Matsumoto, H., Dmitriev, A. V., Kunitsyn, V. E., Andreeva, E. S., et al. (2014). Low-latitude ionospheric effects of energetic electrons during a recurrent magnetic storm, J. *Journal of Geophysical Research: Space Physics*, *119*, 9283–9302. https://doi.org/10.1002/2014JA020349

Taori, A., Patra, A. K., & Joshi, L. M. (2011). Gravity wave seeding of equatorial plasma bubbles: An investigation with simultaneous *F* region, *E* region, and middle atmospheric measurements. *Journal of Geophysical Research*, *116*, A05310. https://doi.org/10.1029/2010JA016229

Tulasi Ram, S., Balan, N., Veenadhari, B., Gurubaran, S., Ravindran, S., Tsugawa, T., et al. (2012). First observational evidence for opposite zonal electric fields in equatorial E and F region altitudes during a geomagnetic storm period. *Journal of Geophysical Research*, *117*, A09318. https://doi.org/10.1029/2012JA018045

Wan, X., Xiong, C., Rodriguez-Zuluaga, J., Kervalishvili, G. N., Stolle, C., & Wang, H. (2018). Climatology of the occurrence rate and amplitudes of local time distinguished equatorial plasma depletions observed by Swarm satellite. *Journal of Geophysical Research: Space Physics*, *123*, 3014–3026. https://doi.org/10.1002/2017JA025072

Xiong, C., Lühr, H., & Fejer, B. G. (2015). Global features of the disturbance winds during storm time deduced from CHAMP observations. *Journal of Geophysical Research: Space Physics*, *120*, 5137–5150. https://doi.org/10.1002/2015JA021302

Xiong, C., Lühr, H., Ma, S. Y., Stolle, C., & Fejer, B. G. (2012). Features of highly structured equatorial plasma irregularities deduced from CHAMP observations. *Annales Geophysicae*, *30*(8), 1259–1269. https://doi.org/10.5194/angeo-30-1259-2012

Xiong, C., Park, J., Lühr, H., Stolle, C., & Ma, S. Y. (2010). Comparing plasma bubble occurrence rates at CHAMP and GRACE altitudes during high and low solar activity. *Annales Geophysicae*, *28*(9), 1647–1658. https://doi.org/10.5194/angeo-28-1647-2010

Yadav, S., Das, R. M., Dabas, R. S., Subrahmanyam, P., & Gwal, A. K. (2011). Response of low-latitude ionosphere of the Indian region during the supergeomagnetic storm of 31 March 2001. *Journal of Geophysical Research*, *116*, A08311. https://doi.org/10.1029/2010JA016373

Yeh, H. C., Su, S. Y., & Heelis, R. A. (2001). Storm time plasma irregularities in the pre-dawn hours observed by the low-latitude ROCSAT-1 satellite at 600 km. *Geophysical Research Letters*, *28*(4), 685–688. https://doi.org/10.1029/2000GL012183

Yeh, H. C., Su, S. Y., Yeh, Y. C., Wu, J. M., Heelis, R. A., & Holt, B. J. (1999). Scientific mission of the IPEI payload on board ROCSAT-1, TAO supplementary issue, 19-42.

Yokoyama, N., & Kamide, Y. (1997). Statistical nature of geomagnetic storms. *Journal of Geophysical Research*, *102*(A7), 14215–14222. https://doi.org/10.1029/97JA00903

Zhang, R., Liu, L., Le, H., Chen, Y., & Kuai, J. (2017). The storm time evolution of the ionospheric disturbance plasma drifts. *Journal of Geophysical Research: Space Physics*, *122*, 11,665–11,676. https://doi.org/10.1002/2017JA024637